Available online at www.sciencedirect.com
ScienceDirect
Icarus 185 (2006) 395–402
ICARUS
www.elsevier.com/locate/icarus

# Observations of Mercury's exosphere: Spatial distributions and variations of its Na component during August 8, 9 and 10, 2003

F. Leblanc [a,*,1], C. Barbieri [b], G. Cremonese [c], S. Verani [b], R. Cosentino [d], M. Mendillo [e], A. Sprague [f], D. Hunten [f]

[a] *Service d'Aéronomie du CNRS, Route des gatines, BP 3, 91371 Verrières-Le-Buisson, France*
[b] *Department of Astronomy, University of Padova, I-35122 Padova, Italy*
[c] *Astronomical Observatory of Padova, INAF, I-35122 Padova, Italy*
[d] *Telescopio Nazionale Galileo, INAF, 38700 Santa Cruz de La Palma, TF, Spain*
[e] *Center for Space Physics, Boston University, MA 02215, USA*
[f] *Lunar and Planetary Laboratory, University of Arizona, Tucson, AZ 85721, USA*

Received 7 March 2006; revised 2 August 2006

Available online 20 October 2006

**Abstract**

Following the observations of August 2002 [Barbieri, C., Verani, S., Cremonese, G., Sprague, A., Mendillo, M., Cosentino, R., Hunten, D., 2004. Planet. Space Sci. 52, 1169–1175], the high resolution spectrograph of the 3.5-m Galileo National Telescope (TNG) has been used to obtain several spatially resolved spectra of Mercury's Na-D on the evenings of 8, 9 and 10 August 2003. The resolution of the spectrograph was 115,000, the slit dimensions were $0.4'' \times 27''$. With respect to Paper I, the planet was in a fairly similar orbital configuration, being at a geocentric distance of approximately 1 AU, and having a True Anomaly Angle (TAA) from 163°–168° instead of 171°–174°. We present here a significantly larger set of observations and discuss several important features regarding the formation of Mercury's sodium exosphere, in particular the role of photon stimulated and thermal desorptions, as well as of the solar wind sputtering and micro-meteoroid vaporization. Thanks to the very good seeing of these observations, we also report and discuss the origins and variations of equatorial structures in Mercury's early morning sodium exosphere.


*Keywords:* Mercury, atmosphere; Spectroscopy; Magnetospheres; Solar wind

## 1. Introduction

The existence of an atmosphere around Mercury was discovered by the Mariner 10 spacecraft, which revealed UV emissions of three atomic elements: H, He and O (Broadfoot et al., 1976). Three other elements (Na, K and Ca) were later discovered with ground-based observations in the visible (Potter and Morgan, 1985; Potter and Morgan, 1986; and Bida et al., 2000, respectively). Due to the low surface number density (approximately $n = 10^5$ atoms/cm$^3$, $P = 10^{-12}$ bar, on the dayside), the atmosphere is collisionless. Therefore, the whole atmosphere is comparable with an exosphere having the exobase coincident with the planet's surface.

To provide more data to understand the complex phenomena observed in the optical and radar domains, we have undertaken observations of the Na exosphere with the high resolution spectrograph (SARG) mounted on the 3.5-m Telescopio Nazionale Galileo (TNG) in the Canary Islands. The advantages of using the TNG in this context come from the good collecting aperture, from the outstanding image quality of the site and of the telescope, and from the excellent performances of the SARG in terms of efficiency and resolution. The present paper greatly expands on the results obtained in the first, largely exploratory attempt to reach this goal (Barbieri et al., 2004; hereafter Paper I), and compares the observations with the model of Leblanc and Johnson (2003). The results are promising enough to plan a program of observations for the next several years. Not only

* Corresponding author. Fax: +39 040 30 94 18.
*E-mail address:* francois.leblanc@aerov.jussieu.fr (F. Leblanc).
[1] Present address: Osservatorio Astronomico di Trieste, Via Tieppolo 11, 34131 Trieste, Italy.

0019-1035/$ – see front matter 
doi:10.1016/j.icarus.2006.08.006

do we hope to clarify the relative roles of the source mechanisms at the origin of Mercury's sodium exosphere, but we also hope to provide a useful data bank for the MESSENGER and Bepi-Colombo space missions.

## 2. Observations and data reduction

Table 1 gives the main characteristics of the SARG spectrograph. For further information on SARG see http://www.pd.astro.it/sarg/. We have equipped it with a 60-Å wide Na filter specifically for the purpose of studying the diffuse Na in Solar System objects (planets, moons, comets, etc.), because it allows a long slit (26.7 arcsec) to be kept on the sky, removes order overlapping, and permits an accurate subtraction of the night sky continuum. Furthermore, the Na filter is placed before the slit, so that the seeing on the slit itself is determined by a narrow wavelength range.

The observations discussed here were carried out on three evenings: 8, 9 and 10 August 2003 between 19:00 and 20:00 UT, namely with the Sun slightly above or just below the horizon, the minimum allowed elevation of the TNG being 13.5°. To save read-out time, the slit was 2x-binned in the spatial direction, making the effective spatial pixel of 0.32 arcsec, approximately 1/20th of the planet's disk. The disk of the planet was indeed spatially resolved with good detail, with a seeing sigma varying from 1.0″–1.4″ and 1.2″–1.6″ the first two nights to 1.2″ the third night. Seeing sigma $\sigma$ is defined in Eq. (1) of Sprague et al. (1997) and is equal to the half width at the $1/e$ point of a two dimensional Gaussian. It is equal to the Full Width Half Maximum (FWHM) divided by 1.67 (Sprague et al., 1997). Table 2 gives the observing conditions for Mercury on these nights.

On the evenings of August 8 and 9, the slit was maintained parallel to Right Ascension (PA = 90°), and placed at several positions across and outside the planet's disk. Many spectra were obtained with exposure times ranging from 60 to 90 s. On August 10, the slit was instead placed along the declination (PA = 0°), and again, several spectra were obtained with exposure times ranging from 60 to 90 s. The main source of noise is due to the varying sky background because of different Sun elevation and illumination inside the dome. The ratio between Mercury emission and the sky background intensities varies between 0.2 and 5.8, between 0.04 and 5.6 and between 0.02 and 5.7 during the first, second and third evenings, respectively. The data set discussed in details in the following has been obtained for value of this ratio larger than one.

Table 1
SARG main parameters

| | |
|---|---|
| Spectrograph resolution | 115,000 |
| Slit length and width | 26.7 × 0.40 arcsec |
| Pixel dimension and scale | 0.022 Å, 0.16 arcsec |
| CCD dimension | 2 K × 4 K pixels |

## 3. Analysis of the spectra

Sample plots of the spectra for two different slit orientations across the center of the planet are shown in Fig. 1.

The conversion of non-calibrated data to Rayleigh emission in Rayleighs (R) has been performed with a method due to Sprague et al. (1997) and which is similar to the method used by Potter et al. (2006). The surface rough-reflectance at Mercury's surface is calculated from the Hapke model (Hapke, 1986) at each location in the surface grid, taking into account the particular geometry and seeing of each observation. The grid-size can be chosen to represent the parameters of the spectrograph (in this case a spatial pixel of 0.32 arcsec). The Hapke reflectance value can then be used to absolutely calibrate the data using the measured continuum in a wavelength range close to the sodium D lines. As an example, Fig. 2 displays the position of the slit on Mercury's disk for spectrum n°43 obtained the third night (Fig. 1b), on an image of the reflectance as calculated by Hapke's model. The $x$-axis is along the planet's equator, positive toward West in the planetocentric frame of reference (namely, the Sun is on the positive $x$ direction). The $y$-axis is along the planet's rotation axis, positive toward its North pole. The position along the slit of the maximum of the calculated reflectance is indicated by the large white cross. This maximum corresponds theoretically to the maximum value of the measured continuum along the slit. Using a typical value for the solar flux around the D1 and D2 lines, it is then possible to associate the number of ADU (Analog to Digital Unit) of the maximum value of the measured continuum to the flux of photons reflected at Mercury's surface towards the observer according to Hapke's model. We have also used the Sprague et al. (1997) approach to calculate the equivalent column density (in number of Na atoms/cm$^2$).

The extraction of the exospheric emission is done by fitting the D1 and D2 solar Fraunhofer lines with a Voigt profile (Hum-

Table 2
Mercury's parameters

| Parameters | August 8, 2003 | August 9, 2003 | August 10, 2003 |
|---|---|---|---|
| Sun–Mercury distance (AU) | 0.463 | 0.464 | 0.465 |
| Illuminated fraction | 59% | 58% | 56% |
| Angular diameter (arcsec) | 6.8 | 6.9 | 7.0 |
| Mercury–Earth radial velocity | −24.5 km/s | −24.6 km/s | −24.7 km/s |
| Mercury–Sun radial velocity | 2.6 km/s | 2.2 km/s | 1.7 km/s |
| Sun–Earth–Mercury phase angle | 79.7° | 81.2° | 82.8° |
| True anomaly angle (TAA) | 163° | 165° | 168° |
| Sub-Earth point (west longitude and latitude) | 150.8°, +7.2° | 155.7°, +7.3° | +160.7°, +7.4° |
| Sub-Solar point (west longitude and latitude) | +71.3°, +0.0° | −74.5, +0.0° | +77.9°, +0.0° |

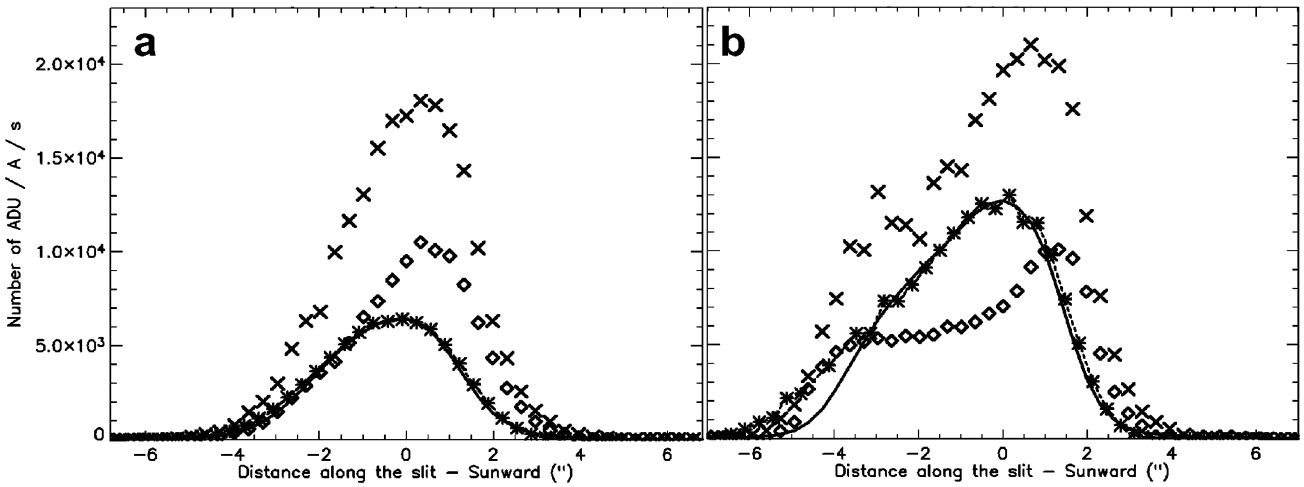


Fig. 1. Examples of tracings of the spectra obtained with the slit across the center of the planet, respectively in PA = 90° (left panel; slit along Right Ascension, orientation celestial E–W, the illuminated bright limb is on the right, slit position n°68) and PA = 0° (right panel; slit along declination, orientation celestial N–S, positive axis points to celestial North pole, slit position n°43). Solid line: measured continuum. Diamonds: measured D1 emission intensity. Crosses: measured D2 emission intensity. Dashed line with stars: Hapke reflectance model (normalized to the maximum of the measured continuum).

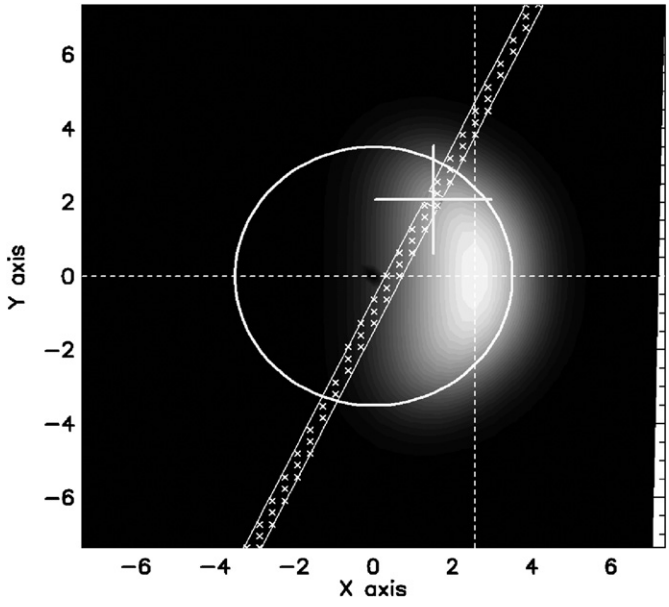


Fig. 2. Hapke reflectivity for slit position n°43 with seeing sigma = 1.2″, the slit position is represented by the two parallel lines with small crosses in it (showing the grid points of Hapke model). The large cross is the position in the slit where the reflectance is maximal.

mer, 1962). Such an approach is particularly needed (rather than a linear interpolation of the solar line as done in Paper I, see Fig. 1, bottom panel, of Paper I) when Mercury's heliocentric radial velocity is small. Indeed, in such a case the exospheric lines fall within the minimum of the solar line. A simple linear interpolation would lead to a significant underestimate of the emission brightness. The continuum value is estimated close to the D1 and D2 emission lines. The seeing value for each slit position is determined by comparing the Hapke reflectivity model along the slit (Fig. 2) with the observed one as illustrated in Fig. 1 (here with a seeing sigma equal to 1.2″). Table 3 gives the seeing sigma range and g-factors for the 3 nights. g-Factor calculation is based on the assumption of a constant solar flux around the D1 and D2 wavelengths during the 3 nights. It supposes a non-active solar period which is also confirmed by the F10.7 solar index from daily average National Geophysics Data Center.

The exact position of the slit is determined by considering that the position perpendicular to the length of the slit is accurately given by the instrument pointing with an uncertainty of ±0.5″ and by considering the seeing effect calculated for each slit position. In order to place the middle of the slit on the disk, we used the fact that the position of the maximum value of the measured continuum should correspond to the theoretical maximum of the reflectance deduced, i.e., from the Hapke model (large white cross in Fig. 2). When these two positions are determined, the middle of the slit can be placed on Mercury's disk. This method is derived from Sprague et al. (1997). The measured brightness of the signal has an uncertainty which is the sum of the instrumental and statistical noises and of the error due to the fit of the solar Fraunhofer line by a Voigt profile. The total uncertainty is estimated to be equivalent to less

Table 3
PSF seeing values and g-factors for the different nights

| Date | Seeing sigma (″) | Seeing FWHM (″) | Sun–Mercury radial velocity (mA) | Earth–Mercury radial velocity (mA) | g-Factor D2 | g-Factor D1 |
|---|---|---|---|---|---|---|
| 08/08/2003 | 1.0–1.4 | 1.7–2.3 | 51.8 | −482 | 3.00 | 2.2 |
| 09/08/2003 | 1.2–1.6 | 2.0–2.7 | 42.6 | −484 | 2.72 | 1.84 |
| 10/08/2003 | 1.2 | 2.0 | 32.9 | −485 | 2.54 | 1.63 |

than 50 kR (i.e., roughly 1000 ADU/A/s). The uncertainty provided by the calibration method must be added when comparing observations of two different nights. It has been calculated by Domingue et al. (1997) as being of the order of 35%. The best set of free parameters which are the exact position of the slit and the seeing sigma, is then derived in order to fit the theoretical Hapke reflectivity profile for each slit position and such that the calibration factor for the whole set of slit positions during one evening remains constant within few tens of percent of the average value

## 4. Discussion of the observations

Fig. 3 displays the global images obtained during each night derived from the successive slit positions (8 sequences of observation during the first night chronologically numbered from 62 to 69, 15 sequences during the second night numbered from 15 to 29 and 11 sequences during the third night numbered from 35 to 45). The seeing sigma during the three nights is equal to $\sim 1.2''$ or $\sim 0.3$ $R_M$ (Mercury radii) for the first and last nights and to $\sim 1.6''$ or $\sim 0.5$ $R_M$ for the second night. The seeing effect is therefore of a very good quality with respect to previous observations of Mercury's exosphere. As an example, Potter et al. (2006) obtained observations with seeing sigma between $1.2''$ and $3''$ and Sprague et al. (1997) reported observations with seeing sigma between 1.5 and $3''$. The spatial distribution of the emission during the first two nights is similar, as shown in panels a and b with a maximum of the brightness close to the subsolar point. For all the slit positions, such a maximum is placed slightly before the limb (or the subsolar line) and close to equatorial regions, but at a distance to the subsolar line smaller than the uncertainty due to uncertainty on the exact slit position and due to the seeing effect. No peak at high latitude is seen in any of the three nights of observation.

Fig. 4 provides the emission brightness distribution along the slit as observed for different positions of the slit during each night. In particular, panel a displays the measured signal for two slit positions covering the same region of the disk but taken 15 min apart during the first night of observation. The observation numbered 63 has been obtained with a seeing sigma equal to $1''$ whereas the observation numbered 68 with a seeing sigma equal to $1.4''$. Considering this difference

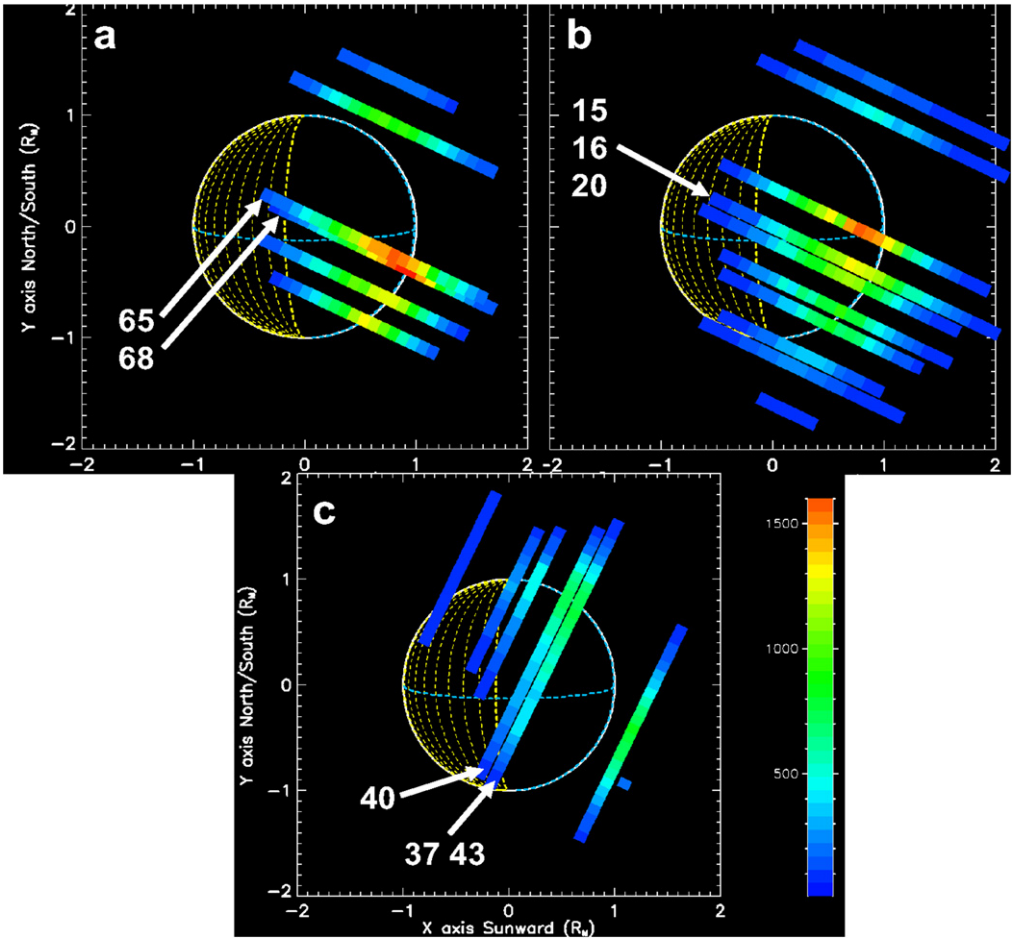


Fig. 3. View of the observations performed during August 2003. On each figure we plotted the brightness of the D2 emission measured along the slit (in kR). All the different positions of the slit are represented (when overlapping of different slit positions occurs, we plotted the average measured signal, the case of slits n°65 and 68, n°15, 16 and 20, and n°40 and 43). The scale of the intensity is the same for each of the nights (scale bar on the right of panel c). Panel a: August 8, 2003. Panel b: August 9, 2003. Panel c: August 10, 2003. On each panel, we plotted the position of Mercury's disk. The Sun is on the right. The nightside of the planet corresponds to the part of the disk with dashed lines and the terminator to the thickest dashed line. The subsolar line is at the limb on the right of each figure. The numbers refer to specific slit position numbers to be discussed in the text.

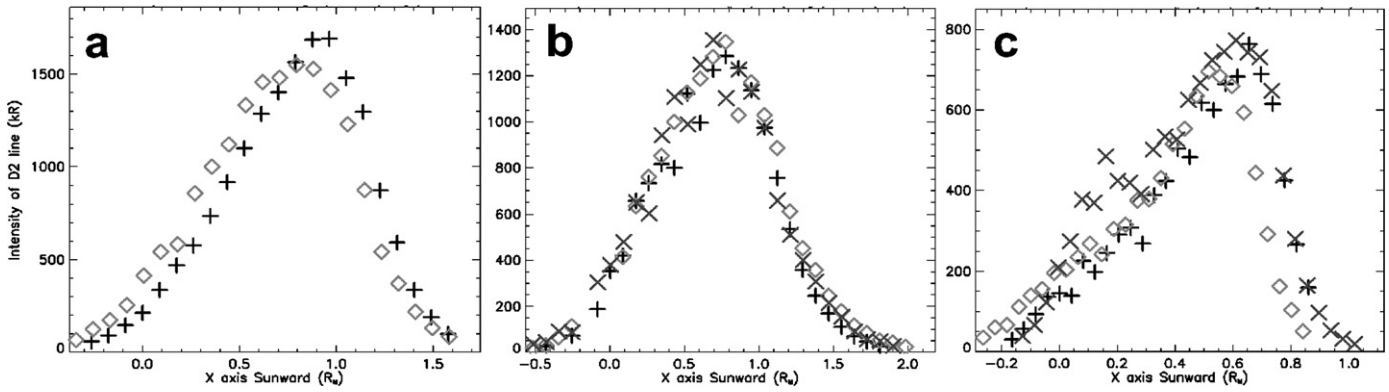


Fig. 4. Measured emission brightnesses: panel a: August 8, 2003, two different times (slit positions n°63, plus, and n°68, diamonds); panel b: August 9, 2003, three different times (slit positions n°15, plus, n°16, diamonds, and n°20, crosses); panel c: August 10, 2003, three different times (slit positions n°37, plus, n°40, diamonds, and n°43, crosses). The corresponding slit positions are indicated in Fig. 3.

in seeing effect, Fig. 4a illustrates how remarkably stable the exosphere seems to be between these two observations. Panel b provides the emission brightness measured for the same slit position than panel a during the second day. The seeing sigma was equal to 1.6″ during the three observations displayed in this latter panel. Panel b shows the same characteristics of a sodium exospheric emission peaking close to the subsolar regions and almost constant during three non-consecutive observations (here separated by 18 min). Fifteen or eighteen minutes correspond to a very short time with respect to Mercury's local time (it is equivalent to ∼5 s of Mercury day), but it is also comparable to the ballistic time of a Na atom ejected from Mercury's surface with a 1.5 km/s velocity (that is the typical velocity of ejection associated with most of the known mechanisms of ejection). Thus, such a brightness pattern could not have been produced by a transient event occurring at the beginning of the set of observations (which excludes, as an example, a large meteoroid impact or a solar-induced event). It must have been produced either by photon stimulated desorption, thermal desorption, micro-meteoroid impact or solar wind sputtering (see Killen et al., 1999, or Leblanc et al., 2006, for details on these processes). The peak of the signal observed during both nights (Figs. 3a and 3b) is close to the subsolar point within the position uncertainty associated to the seeing effect that is between 1/3 and 1/2 of $R_M$. Mercury's magnetosphere is thought to be a dynamo type magnetosphere and is therefore thought to have open magnetic field line regions leading to the sputtering of Mercury's surface preferentially at high latitude and centered on the subsolar line (Ip and Kopp, 2002; Kallio and Janhunen, 2003). Several parameters can influence the geometry of the sputtered regions in particular the components of the Interplanetary Magnetic Fields (Sarantos et al., 2001). However, following the numerous studies of the role of the solar wind sputtering, only a strong solar dynamic pressure can lead to the sputtering of the subsolar regions. Such a situation has been discussed as potentially occurring at Mercury, but less than a few percent of the time (Siscoe and Christofer, 1975; Hood and Schubert, 1979; Goldstein et al., 1981). In the case of micro-meteoroid vaporization, the expected spatial distribution of the signal should not display such a maximum close to the subsolar point (Cremonese et al., 2005; Marchi et al., 2005). Therefore, it is most probable that the observed spatial distribution of the emission brightness is due to either photon stimulated desorption or thermal desorption.

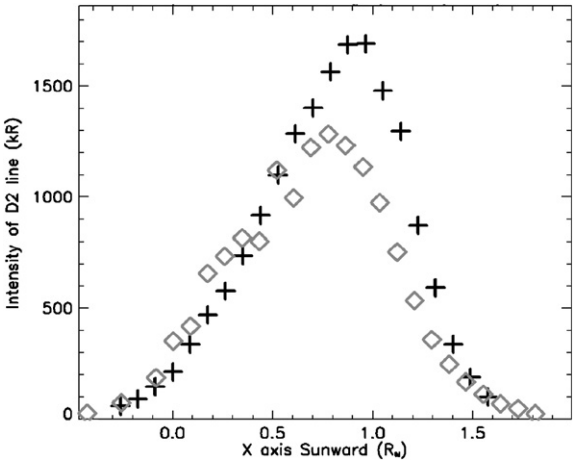


Fig. 5. Comparison of the brightness measured along the slit placed at the center of the disk, the 8th and 9th (same as panels a and b, Fig. 4, slit position n°68 and n°15).

Because panels a and b in Fig. 4 display the measured signal for essentially the same slit positions (within the uncertainty on the slit position) during the August 8 and 9 nights, we also compare these measurements. Fig. 5 displays the result of such comparison, which clearly shows that the spatial distribution of the emission brightness, as well as the total brightness of the signal are very similar, despite a higher seeing value and smaller sky—Mercury exospheric intensities during the second night of observation. Therefore the observed stability of the distribution of the emission between these two nights suggests that the observed sodium exosphere during these two nights has been mainly produced by mechanisms stable during one Earth day like photon sputtering and thermal desorptions rather than mechanisms like solar wind sputtering variable on short time scale.

Panel c of Fig. 4 displays the emission brightness observed during three consecutive slit positions during the third night, separated by 8 min between the two first observations, and by 10 min between the two last observations. The 'diamond'

symbols correspond to the second observation obtained slightly more southern than the two others (see Fig. 3c), the 'plus' to the first and the 'crosses' to the third (also displayed Fig. 1b). These slit positions are almost perpendicular to those of Figs. 4a and 4b. The observed distribution of the signal along the slit is significantly different from the ones displayed in panels a and b. It is probably due, first of all, to the difference in the orientation of the slit. However, panel c clearly suggests the presence of a second peak or plateau in the emission brightness close to the terminator at equatorial latitudes (also visible in Fig. 3, panel c). The maximum of the emission brightness along the slit (at $X = 0.5\ R_M$) remains close to the limb. It changes by only 15% between the first and the second observations (which may be related to the slight difference in the position of the slits), and is constant between the second and third slit positions. The variation of the second peak or plateau during the third observation is therefore short in time with respect to Mercury's time scale and should be associated to a localized event leading to a sudden and localized increase of the flux of sodium atoms ejected from the surface. It is less evident in the emission brightness associated to the D1 line (see Fig. 1b), but is above instrumental and calibration uncertainties in the case of the D2 line emission brightness. Instrumental, statistic and sky noises are all estimated to lead to a total emission brightness uncertainty around 50 kR. The ratio between the useful signal and the sky background was equal to 1, 1.9 and 5.7 for the observations numbered 37, 40 and 43, respectively. The seeing sigma evaluated for each slit position was very stable during the whole evening and equal to 1.2″. Unfortunately, no consecutive observation with a slit placed close to this one has been done afterward.

The apparent size along the slit of this increasing second peak is less than 0.6 $R_M$ as shown by Fig. 6, whereas the seeing for this night was ∼0.3 $R_M$. The total increase in the D2 emission brightness along the slit is of the order of 2000 kR. Such an increase corresponds to a total increase of the column density by $\sim 8 \times 10^{11}$ Na/cm$^2$ (using optically thin assumption and the g factor given in Table 3). If the event leading to this increase started 10 min earlier (that is, just after the observation corresponding to the diamonds of Fig. 4c), it would imply an ejection rate of new sodium atoms in Mercury's exosphere of at least $\sim 10^8$ Na/cm$^2$/s, and even larger if the position of the source at Mercury's surface is outside the slit viewing or if the event started less than 10 min before. Such ejection rate is much larger than the rate of ejection due to micro-meteoroid impact vaporization, which has been estimated to be equal to $\sim 5 \times 10^5$ Na/cm$^2$/s (Killen et al., 2004), and even less, $\sim 2 \times 10^4$ Na/cm$^2$/s, according to Cremonese et al. (2005), a value later corrected to $\sim 2.1 \times 10^6$ Na/cm$^2$/s (Cremonese et al., 2006). It is also much larger than the rate of ejection due to solar wind sputtering, estimated equal to $\sim 5 \times 10^6$ Na/cm$^2$/s (Killen et al., 2004). A large meteoroid impact or a short and significant increase in the micro-meteoroid flux is possible but also unlikely, given the low probability for such an impact to occur at Mercury (Marchi et al., 2005). A variation of the micro-meteoroid flux by more than a factor 50–200 is also very unlikely at Mercury's orbit. Solar wind sputtering can be at the origin of this event, if the solar wind flux reaching the surface is increased by at least a factor 20 which can be produced by an increase of the solar flux or/and by the area of Mercury's surface bombarded by solar wind particles.

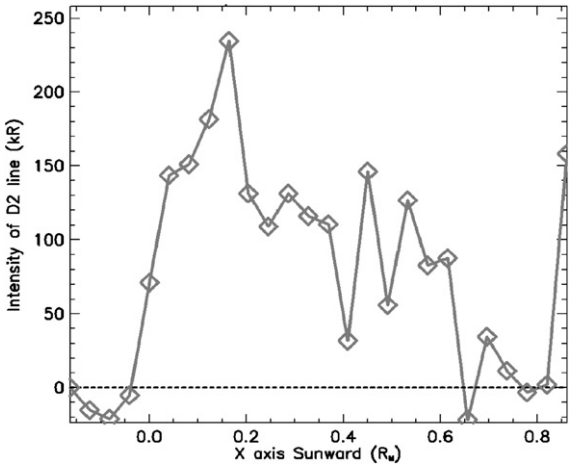


Fig. 6. Increase of the measured D2 emission brightness along the slit between the measurement corresponding to the crosses (slit position n°37) and the measurement corresponding to the diamonds (slit position n°43) in Fig. 5c. This result has been obtained by simply subtracting both measured emission brightnesses.

A second possibility to consider is that the surface concentration of Na in Mercury's upper surface is larger than the 0.0053 value supposed by Killen et al. (2004). Actually, Cremonese et al. (2005) suggested that the Na concentration could be rather equal to 0.037. Moreover, an early morning increase of the surface density has been suggested by Leblanc and Johnson (2003) in relation with the day-to-nightside migration of the exospheric volatiles. Their Plate 1 provides typical upper surface density in Na/cm$^2$. In particular, close to the aphelion (that is, corresponding to the present set of observations), these authors suggest that at the equator the early morning upper surface density could reach $\sim 10^{13.5}$ Na/cm$^2$, which would correspond to a concentration of 0.04 using a surface density of $7.5 \times 10^{14}$ atoms/cm$^2$ (there is an error in Leblanc and Johnson, 2003, page 270 regarding the range of variation of the surface concentration, which has to be read as between 0.05 and 0.003). A concentration of the order of 0.037–0.04 would therefore induce an ejection rate by solar wind sputtering close to what we estimate as needed in order to produce the observed feature displayed in Figs. 4c and 6.

Photon stimulated and thermal desorption could produce localized peak in Mercury's exosphere at such an early local time by the rising of the Sun on a crater having part of its slope facing the Sun, as it has been already reported by Sprague et al. (1997). The maximum ejection rate for photon stimulated desorption has been estimated by Killen et al. (2004) as being equal to $\sim 10^7$ Na/cm$^2$/s at the subsolar point, if the concentration of Na in Mercury's upper surface is equal to 0.0053. Therefore, a 10 times larger concentration should be sufficient to produce the ejection rate suggested by this observation. However, a time scale of 10 min is incompatible with these two latter processes of ejection. Indeed, 10 min correspond to a rotation

of the Sun around Mercury by less than 1/50°. This is far from being enough to produce a significant change of the solar zenith angle at any place on Mercury's surface.

Transient events such as this are, by their very nature, difficult to study unless observations are conducted far more frequently than is now occurring. Thus, we are left with two possible "standard mechanisms" as possible explanations that are both somewhat unlikely: a very large meteoritic impact or the sputtering of Mercury's surface by solar wind at equatorial early morning latitudes. A third possibility not discussed before is that an unusual change of the circulation of the magnetospheric ions in Mercury's magnetosphere (as an example induced by a change of the Interplanetary Magnetic Field direction, see Luhmann et al., 1998) might have produced locally an increase of the ion flux reimpacting the surface and a subsequent ejection of Na atoms. However, in order to produce such an ejection rate, the magnetospheric ion population would need to be much larger than commonly thought (see as an example the effect of the $Na^+$ population in Leblanc et al., 2003).

Hunten and Wallace (1993) have developed a method to convert emission brightness to a corresponding column density of sodium atoms for any value of the optical thickness. Unfortunately, this method is essentially valid for observations done above Mercury's disk, and cannot be used to calibrate the off limb part of the observations. This method has been extensively used by Sprague et al. (1997). It provides in general a larger value for the column density when using the D2 emission brightness than the D1 one (by a factor between 1 and 5 most of the time). As underlined by Killen and Ip (1999), this may be due to the assumption of a Na exosphere thermally accommodated to the surface which implies an overestimate of the optical thickness of the D1 and D2 lines if the Na population is hotter than the surface. We adapted the model described in Leblanc and Johnson (2003) and Leblanc et al. (2003) for the same heliocentric positions and geometry of the observations (phase angle, ecliptic inclination of Mercury's axis and seeing effects). No change was made in the parameters of the simulation already described in these papers (same meteoroid flux, same parameter for the solar wind and solar photon flux, same surface temperature...). Observations and simulations provide a range of column density in relatively good agreement (within a factor 3). The main difference is that the position of the maximum is much closer to the subsolar point in the observations than in the simulations (Leblanc and Johnson, 2003), and that this maximum is three times larger than the maximum column density in the simulations. Clearly, the simulation predicts a release of the sodium atoms too early in the morning with respect to the observations. In the simulation, the ejection rate produces a maximum of column density at the center of the visible part of Mercury's disk. This seems to indicate that the depletion of the surface in the morning predicted by Leblanc and Johnson (2003) does not occur as early as supposed.

One solution for this discrepancy is that thermal desorption, the main process leading to this early release of the surface sodium atoms, is not as efficient as supposed in Leblanc and Johnson (2003). As an example, it has been suggested by Sprague (1992) that diffusion through the grains should supply fresh sodium atoms to the upper surface on timescales of several Earth days. In the same way, diffusion through the pores of the regolith should be also a source of fresh sodium atoms during part of the morning. Potter et al. (2006) reported that the ratio between the observed emission at the limb and the observed emission at the dawn terminator reaches a minimum at Mercury's aphelion as well as at Mercury's perihelion. These authors concluded that it is in contradiction with the prediction of an exosphere strongly influenced by the terminator velocity which would have produced a strong dawn terminator signature at aphelion. However, this strong terminator signature is essentially due to the role of the thermal desorption in depleting the surface in volatiles as soon as the surface temperature reaches values above 400 K which has been supposed in the model of Leblanc and Johnson (2003). Actually, if thermal desorption depletes the surface less efficiently at temperature around 400 K than supposed by Leblanc and Johnson (2003) but remains efficient for larger temperature, these strong exospheric signatures related to surface depletion should occur closer to the subsolar line at aphelion than at perihelion, the surface temperature varying from a maximum of 700 K at perihelion to a maximum of 550 K at aphelion. Therefore, the lack of significant difference between the dawn terminator and the limb emission intensities at the aphelion reported by Potter et al. (2006) could be simply due to a release of the sodium trapped in Mercury's surface too close to the subsolar region for being spatially distinguishable in Potter et al. (2006) observations.

## 5. Conclusions

A new set of observations of Mercury's sodium exosphere using the SARG/TNG (Barbieri et al., 2004) has been performed during three consecutive nights in August 2003. These observations suggest that photon stimulated desorption and/or thermal desorption are the main processes at the origin of the measured sodium emission brightness during these three nights of observations. In particular we do not see any feature during the first two nights that could be associated to solar wind sputtering (no peak in the exospheric emission at polar latitude nor an extended exosphere above the poles). In the contrary, during the first two nights we observe a sodium exosphere remarkably stable, excluding any transient event. The third night displays a localized feature in the early morning of Mercury which varies on very short time scale with respect to Mercury's diurnal scale. This short time event cannot be explained by localized enhancement in Mercury's sodium exosphere due to either photon stimulated desorption or thermal desorption. Solar wind ion or magnetospheric ion sputtering are the best candidate to produce this short time variation.

A comparison with the simulation by Leblanc and Johnson (2003) displays significant discrepancy, which suggest that processes occur in Mercury's morning that supplies fresh sodium atoms to the upper surface, or that thermal desorption is not as efficient as assumed in that model. Indeed, the maximum intensities of the D1 and D2 emissions are observed significantly closer to the subsolar region than predicted by the model. This discrepancy suggests that the upper surface

depletion in sodium atoms, early in the morning, does not occur as efficiently as described in Leblanc and Johnson (2003) and discussed by Hunten and Sprague (1997). It could also explain the reported discrepancy between Potter et al. (2006) observations and the prediction of this model. Such a surface depletion is, so far, the only available explanation for the global morning/afternoon asymmetry of the sodium exosphere now established by most of the observers of Mercury's sodium exosphere (Sprague et al., 1997; Schleicher et al., 2004; Barbieri et al., 2004; Potter et al., 2006) as well as the apparent maximum of Mercury's exospheric sodium total content at aphelion (Killen et al., 2004).

## Acknowledgments

This work has been partly supported by INAF and by the Europlanet network.

## References

Barbieri, C., Verani, S., Cremonese, G., Sprague, A., Mendillo, M., Cosentino, R., Hunten, D., 2004. First observations of the Na exosphere of Mercury with the high resolution spectrograph of the 3.5 m Telescopio Nazionale Galileo. Planet. Space Sci. 52, 1169–1175.

Bida, T.A., Killen, R.M., Morgan, T.H., 2000. Discovery of calcium in Mercury's atmosphere. Nature 404, 159–161.

Broadfoot, A.L., Shemansky, D.E., Kumar, S., 1976. Mariner 10: Mercury atmosphere. Geophys. Res. Lett. 3, 577–580.

Cremonese, G., Bruno, M., Mangano, V., Marchi, S., Milillo, A., 2005. Release of neutral sodium from the surface of Mercury induced by meteoroid impacts. Icarus 177, 122–128.

Cremonese, G., Bruno, M., Mangano, V., Marchi, S., Milillo, A., 2006. Corrigendum to "Release of neutral sodium atoms from the surface of Mercury induced by meteoroid impacts" [Icarus 177 (2005) 122–128]. Icarus 182, 297–298.

Domingue, D.L., Sprague, A.L., Hunten, D.M., 1997. Dependence of mercurian atmospheric column abundance estimations on surface-reflectance modeling. Icarus 128, 75–82.

Goldstein, B.D., Suess, S.T., Walker, R.J., 1981. Mercury: Magnetospheric processes and the atmospheric supply and loss rate. J. Geophys. Res. 86, 5485–5499.

Hapke, B., 1986. Bidirectional reflectance spectroscopy. 4. The extinction coefficient and the opposition effect. Icarus 67, 264–280.

Hood, L., Schubert, G., 1979. Inhibition of solar wind impingement on Mercury by planetary induction currents. J. Geophys. Res. 84, 2641–2647.

Hummer, D.G., 1962. Non-coherent scattering. I. The redistribution function with Doppler broadening. Mon. Not. R. Astron. Soc. 125, 21–37.

Hunten, D.M., Sprague, A.L., 1997. Origin and character of the lunar and mercurian atmospheres. Adv. Space Res. 19 (10), 1551–1560.

Hunten, D.M., Wallace, L.V., 1993. Resonance scattering by mercurian sodium. Astrophys. J. 417, 757–761.

Ip, W.-H., Kopp, A., 2002. MHD simulations of the solar wind interaction with Mercury. J. Geophys Res. 107 (A11), doi:10.1029/2001JA009171. 1348.

Kallio, E., Janhunen, P., 2003. Solar wind and magnetospheric ion impact on Mercury's surface. Geophys. Res. Lett. 30 (17), doi:10.1029/2003GL017842. 1877.

Killen, R.M., Ip, W.-H., 1999. The surface-bounded atmospheres of Mercury and the Moon. Rev. Geophys. 37, 361–406.

Killen, R.M., Potter, A.E., Fitzsimmons, A., Morgan, T.H., 1999. Sodium D2 line profiles: Clues to the temperature structure of Mercury's exosphere. Planet. Space Sci. 47, 1449–1458.

Killen, R.M., Sarantos, M., Potter, A.E., Reiff, P.H., 2004. Source rates and ion recycling rates for Na and K in Mercury's atmosphere. Icarus 171, 1–19.

Leblanc, F., Johnson, R.E., 2003. Mercury's sodium exosphere. Icarus 164 (2), 261–281.

Leblanc, F., Delcourt, D., Johnson, R.E., 2003. Mercury's sodium exosphere: Magnetospheric ion recycling. J. Geophys. Res. Planets 108 (E12), doi:10.1029/2003JE002151. 5136.

Leblanc, F., Chassefière, E., Johnson, R.E., Hunten, D.M., Kallio, E., Delcourt, D.C., Killen, R.M., Luhmann, J.G., Potter, A.E., Jambon, A., Cremonese, G., Mendillo, M., Yan, N., Sprague, A.L., 2006. Mercury's exosphere origins and relations to its magnetosphere and surface. Planet. Space Sci. In press.

Luhmann, J.G., Russell, C.T., Tsyganenko, N.A., 1998. Disturbances in Mercury's magnetosphere: Are Mariner 10 "substorms" simply driven? J. Geophys. Res. 103, 9113–9119.

Marchi, S., Morbidelli, A., Cremonese, G., 2005. Flux of meteoroid impacts on Mercury. Astron. Astrophys. 431, 1123–1127.

Potter, A.E., Morgan, T.H., 1985. Discovery of sodium in the atmosphere of Mercury. Science 229, 651–653.

Potter, A.E., Morgan, T.H., 1986. Potassium in the atmosphere of Mercury. Icarus 67, 336–340.

Potter, A.E., Killen, R.M., Sarantos, M., 2006. Spatial distribution of sodium on Mercury. Icarus 181, 1–12.

Sarantos, M., Reiff, P.H., Hill, T.W., Killen, R.M., Urquhart, A.L., 2001. A Bx-interconnected magnetosphere model for Mercury. Planet. Space Sci. 49, 1629–1635.

Schleicher, H., Wiedemann, G., Wöhl, H., Berkefeld, T., Soltau, D., 2004. Detection of neutral sodium above Mercury during the transit on 2003 May 7. Astron. Astrophys. 425, 1119–1124.

Siscoe, G.L., Christofer, L., 1975. Variations in the solar wind standof distance at Mercury. Geophys. Res. Lett. 2, 158.

Sprague, A.L., 1992. Mercury's atmospheric bright spots and potassium variations: A possible cause. J. Geophys. Res. 97, 18257–18264.

Sprague, A.L., Kozlowski, R.W.H., Hunten, D.M., Schneider, N.M., Domingue, D.L., Wells, W.K., Schmitt, W., Fink, U., 1997. Distribution and abundance of sodium in Mercury's atmosphere, 1985–1988. Icarus 129, 506–527.